Journal of Energy Storage 60 (2023) 106681

Contents lists available at ScienceDirect

Journal of Energy Storage

journal homepage: www.elsevier.com/locate/est

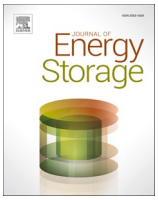

Research papers

Battery sizing of 48 V plug-in hybrids considering calendar and cycle degradation☆

Tobias Frambach [a,b], Ralf Liedtke [a], Egbert Figgemeier [b,c,*]

[a] Robert Bosch GmbH, Robert-Bosch-Straße 2, 71701 Schwieberdingen, Germany
[b] Institute for Power Electronics and Electrical Drives (ISEA), RWTH Aachen University, Jägerstraße 17-19, 52066 Aachen, Germany
[c] Helmholtz Institute Münster (HI MS), IEK-12, Forschungszentrum Jülich, Corrensstraße 46, 48149 Münster, Germany

ARTICLE INFO

Keywords:
Plug-in hybrid electric vehicle
48 V
Battery aging
Lifetime model
Real-driving simulation

ABSTRACT

Plug-in hybrid electric vehicles (PHEVs) with battery packs tailored to the driving use case can help to reduce the environmental footprint of the transportation sector. Compared to common high-voltage systems, PHEVs based on a low-voltage level show a higher fuel consumption, but in return benefit from lower component costs and allow the utilization of cheaper high-energy cells. In this paper, the battery size of a 48 V PHEV concept is optimized to minimize the operational costs while taking battery degradation into account and ensure a lifetime-robust system layout. To investigate the applicability of high-energy batteries, 31 automotive-grade cells were investigated experimentally in a calendar and cycle aging study. The results show that calendar aging has a significant contribution of 17.5 % to the overall capacity loss and should be considered during the battery design process. The cycle degradation model is integrated in a Dynamic Programming simulation environment with various real-driving speed and slope profiles, which are extracted from a measured year-round driving profile. The simulation results show, that considering the degradation in the energy management strategy reduces the capacity loss but results in higher operational costs throughout the vehicle lifetime. The extension of a mild hybrid vehicle to a PHEV can reduce the operational costs by 18.5 %. If the vehicle is not charged, the costs increase by 6 % highlighting the need for frequent charging of PHEVs.

1. Introduction

In recent years, vehicles are electrified to reduce fossil fuel consumption by increasing the share of electric energy. Hybrid electric vehicles (HEVs) gain electric energy by brake energy recuperation or load shifting of the internal combustion engine [1]. Plug-in hybrid electric vehicles (PHEVs) have an additional charge plug to use electrical grid energy and increase the electric driving share further [2]. While larger battery pack capacities provide the opportunity to reduce the fuel consumption, the higher component prices increase the total costs over the vehicle lifetime. Optimal sizing of battery systems for PHEVs is therefore still an existing challenge [3–5], especially due to the coupling with the battery aging behavior and energy management system (EMS) [6].

While HEVs can be operated on a 48 V system voltage level, PHEVs are commonly operated with high-voltage components in the range of 400 V. However, 48 V systems with electric peak powers of up to 30 kW allow the coverage of many driving operations, especially in the lower vehicle segments [7,8]. Measured results of a 48 V PHEV demonstrator vehicle show that this power requirement is sufficient for urban driving situations while CO_2 emissions can be reduced significantly due to the higher electric driving share [9]. Similarly, the life-cycle CO_2 reduction is significantly larger compared to HEVs without a charging opportunity and is close to the possible savings of a high-voltage PHEV [10]. Because low-voltage powertrain components are less expensive and do not require additional safety measures for maintenance, 48 V PHEVs can be a cost-efficient alternative compared to high-voltage PHEVs.

Lithium-ion batteries are typically used to store electrical energy and enable larger shares of electric driving in PHEVs. In 48 V PHEV applications, additional cost savings can be achieved with the utilization of high-energy battery cells. Due to the lower power requirements, the power-to-energy ratio of 48 V PHEVs is close to typical battery electric vehicles (BEVs) applications. The lower price per kWh and production scaling effects of widely used high-energy cells results in lower cell

☆ This paper has not been presented at a conference or submitted elsewhere previously.

* Corresponding author at: Jägerstraße 17-19, 52066 Aachen, Germany.
E-mail address: e.figgemeier@fz-juelich.de (E. Figgemeier).

https://doi.org/10.1016/j.est.2023.106681
Received 13 July 2022; Received in revised form 16 December 2022; Accepted 9 January 2023
Available online 20 January 2023

prices compared to cells for high-voltage PHEV applications [11,12], which need to be adjusted for higher power requirements.

Defining the optimal battery size in PHEVs is a major research topic as the battery accounts for a large share of the overall powertrain costs. The drivetrain components of a parallel PHEV are optimized in [13] with regard to the lowest costs in a convex optimization framework. The authors in [14] investigate the influence of different driving profiles on the cost-optimal battery capacity and demonstrate that the yearly mileage strongly affects the optimization results.

The problem of component dimensioning is often accompanied by the associated optimization of the EMS. Since two energy sources are available in PHEVs, numerous strategies have been developed to find the optimal power share [15]. Next to lowering the fuel consumption or component costs, the optimization target can also include battery degradation. Conequently, studies deal with the design of aging-aware EMSs that include both domains to analyze the trade-off between the two conflicting targets [16,17].

The strategies can generally be divided into rule-based and optimization-based EMSs [18]. Rule-based strategies are easy to implement online and do not require a priori information of the drive cycle. The integration of battery degradation with varying thresholds [19] or a fuzzy logic controller [20,21] demonstrates that rule-based strategies can improve the optimization target. However, rule-based EMSs usually lack optimality and the rules, which are usually not transferable to other powertrain systems, need to be calibrated.

Optimization-based EMSs aim to find the optimal control set of a certain cost function und are commonly divided into offline and online strategies. If the drive cycle information is available a priori, the global-optimal solution can be found. Therefore, offline strategies are typically used to generate benchmark results or to improve other online strategies based on the global-optimal findings. The additional integration of battery degradation has been widely studied in Dynamic Programming (DP) [22,23] and Pontryagin's minimum principle (PMP) [24,25] algorithms. Online EMSs transfer the global-optimization problem into an instantaneous problem and can be implemented online due to their real-time capability. Improvements of the aging-aware objective functions are shown for the Equivalent Consumption Minimization Strategy (ECMS) [26], Model Predictive Control (MPC) [27,28]. The result of a real-time optimization-based EMS is only suboptimal as the equivalent factor needs to be calibrated for the ECMS and the MPC requires an uncertain drive cycle prediction on a certain time horizon.

The battery aging models used for powertrain simulations can be divided into electrochemical and semi-empirical models. Electrochemical models try to accurately describe the chemical processes inside the battery cell. Typically the growth of the solid electrolyte interface (SEI) on the anode surface is calculated, as it is considered the main aging mechanism for usual operation conditions [29]. The capacity loss can be precisely calculated, however electrochemical models are used in few powertrain studies [30] due to long calculation times and intensive model parametrizations. Semi-empirical models are based on simplified formulas that describe the battery degradation as a function of aging-relevant parameters, which are fitted through aging experiments [31]. These models are used in many sizing and EMSs studies because of their simplicity and low calculation time. The models of a commercial LFP cell [32,33] are frequently used in powertrain studies. Nevertheless, the comparison of the aging behavior between studies is often difficult as the experimental procedure is not standardized, the dependency on various aging mechanisms of other cell types is typically unequal and the application type of the cell is different or not specified [34].

To reduce the production costs and strengthen the availability of electric mobility in lower vehicle segments, further research in the field of low-voltage PHEVs is necessary. Only a few studies have investigated this concept and to the best of our knowledge, a battery aging-aware sizing study does not exist. Even though battery aging has been integrated into many high-voltage PHEV powertrain studies, the calendar aging influence is mostly neglected. Furthermore, the presented cycle aging models show differences compared to recent battery aging studies, because a strong dependency on the time spent in charge sustaining mode, which is especially important in PHEV applications, is observed [35]. The widely used degradation models do not consider this effect and are based on commercial high-power cells, contrary to the requirements of 48 V PHEV applications.

To address the mentioned research gaps, this study discusses the battery aging in low-voltage PHEV applications and the derivation of the cost-optimal battery size. The main contributions are as follows: First, experimental results of a conducted aging study of a current automotive high-energy battery cell are presented and compared to a derived semi-empirical aging model. The separation into a cycle and calendar aging model allows to investigate the importance of calendar aging and validate if it can be neglected. Second, the aging model is implemented into a sizing framework using DP to derive a system layout that meets the lifetime requirements, which has not been reported in literature for 48 V PHEVs. Lifetime influencing factors are discussed with various real-driving cycles to ensure a functional system for different customer profiles. Additionally, this contribution sheds light on the trade-off between the battery aging and fuel consumption and elaborates if additional cost savings are possible with an aging-aware EMS. Finally, the cost-optimal battery size is derived with a large database of year-round cycles to ensure a realistic behavior under real-driving conditions and compared to the CO_2-optimal results.

The paper is organized as follows: Section 2 presents the powertrain simulation model and assumptions. The results of the aging study are shown in Section 3. The sizing framework is explained in Section 4. The resulting simulation results are shown and discussed in Section 5. Finally, Section 6 summarizes the findings of this study and open research questions are presented.

2. Vehicle model

2.1. Powertrain description

The investigated system in this study is a parallel hybrid, where the electric machine (EM) is located between the transmission and the internal combustion engine (ICE), also called P2 configuration. Table 1 summarizes the main vehicle parameters.

The ICE can be decoupled, which allows pure electric propulsion of the vehicle. If the required power exceeds the limits of the electric powertrain system or the State of Charge (SoC) is at a lower limit, the ICE is turned on and propels the vehicle in combination with the EM. Electric energy can be gained during recuperation braking conditions and by load shifting of the ICE. The battery is assumed to be fully charged for each driving day.

2.2. Longitudinal dynamics

The required wheel power P_{Whl}, which needs to be satisfied in the utilized backward simulation, is calculated as follows:

Table 1
Main vehicle parameters [10].

Property	Symbol	Value
Vehicle base weight (kg)	m_0	1565
Electric powertrain weight (kg)	$m_{0,\ Edr}$	50
Battery energy density (Wh/kg)	ρ_{Bat}	130
Frontal area (m^2)	A	2.13
Air resistance coefficient	c_w	0.250
Rolling resistance coefficient	f_R	0.008
Equivalent rotational inertia (kgm^2)	Θ	1.1
Gearbox mechanical efficiency	η_{Tra}	0.9
12 V electrical system load (W)	P_{Pnt}	800
Fuel lower heating value (MJ/kg)	Q_{llhv}	42.9

$$P_{Whl} = \left(m_{veh}\frac{dv}{dt}\Theta + m_{veh}gf_R cos(\alpha) + m_{veh}gsin(\alpha) + 0.5c_w A\rho_{Air}v^2 \right) v \quad (1)$$

where m_{veh} is the vehicle weight, v is the vehicle speed, Θ is the equivalent rotational inertia at wheel level, g is the gravitational acceleration, f_R is the tire-rolling resistance coefficient, α the climbing angle, c_w the air resistance coefficient, A the frontal area, and ρ_{Air} the air density. To consider the influence of the increasing battery weight with higher battery capacities, the total weight of the vehicle is defined as

$$m_{veh} = m_0 + m_{0,Edr} + \frac{E_{Bat}}{\rho_{Bat}} \quad (2)$$

where m_0 is the vehicle base weight, $m_{0,\ Edr}$ is the electric powertrain weight without the battery, E_{Bat} is the battery capacity, and ρ_{Bat} is the battery gravimetric energy density. The battery power is then calculated as

$$P_{Bat} = \frac{P_{Whl}}{\eta_{Edr}\eta_{Tra}}\psi_{split} + \frac{P_{Pnt}}{\eta_{DC/DC}} \quad (3)$$

where η_{Edr} is the combined EM/Inverter efficiency, η_{Tra} is the transmission efficiency, ψ_{split} is the power split between the EM and ICE, P_{Pnt} is the 12 V electrical system load, and $\eta_{DC/DC}$ is the converter efficiency between 12 V and 48 V. A charging efficiency of 85 % is considered to obtain the energy from the grid. For power splits $\psi_{split} < 1$ the ICE is turned on and the fuel consumption is calculated as

$$\dot{m}_f = \frac{P_{Whl}}{\eta_{ICE}\eta_{Tra}Q_{lhv}}\left(1 - \psi_{split}\right) \quad (4)$$

where η_{ICE} is the ICE efficiency and Q_{lhv} is the lower heating value of the fuel. The utilized efficiency maps of the ICE η_{ICE} and EM η_{Edr} are shown in Fig. 1.

2.3. Drive cycle generation

PHEVs can drive in charge depleting and charge sustaining mode which influences the energy efficiency and battery aging behavior. Therefore, different driving cycles lead to significantly different optimizations results. Various real-driving trips are simulated in this study to investigate the effects of different driving cycles on the simulation results. The vehicle speed and slope profiles, which are gained by a Global Position System (GPS) map-matching, are recorded during on-the-road measurements to ensure realistic operation conditions. The cycles cover a broad range of distances up to 680 km and include city and highway driving shares. Further insights in the driving dynamics are provided in [10] for the average driver use-case.

2.4. Battery circuit model

The electrical behavior of the battery is modeled with an equivalent circuit model, which considers the open-circuit voltage and internal resistance values of the cell, as follows,

$$I_{Bat} = \frac{U_{OCV} - \sqrt{U_{OCV}^2 - 4P_{Bat}R_{DC,5s}}}{2R_{DC,5s}} \quad (5)$$

$$\dot{SOC} = -\frac{I_{Bat}}{C_{Bat}} \quad (6)$$

where I_{Bat} is the battery pack current, U_{OCV} is the open-circuit voltage, P_{Bat} is the battery pack power, $R_{DC,\ 5s}$ is the internal resistance measured after a 5 s pulse, SOC is the state-of-charge, and C_{Bat} is the battery pack capacity. The open-circuit voltage and internal resistance are adapted from [10].

3. Battery aging model

The battery aging model in this study is based on our own experimental results. Widely used aging models neglect the influence of the Depth of Discharge (DoD) on the degradation [32,33], which is specifically important for PHEVs in charge sustaining mode, where the battery is cycled in a narrow range. Recent aging studies show that the DoD has a major influence on the aging performance [35,36]. Furthermore, our results are based on a large-format 108 Ah battery cell with $LiNi_{0,5}Mn_{0,3}Co_{0,2}O_2$ (NMC532) on the cathode and graphite on the anode, which is suitable for automotive 48 V PHEV applications. All experiments were conducted with Basytech HPS battery cell testers and stored in climate chambers. The battery cells of the cycle aging study are clamped by steel plates with springs which are tightened according to the datasheet requirements. The initial state of charge of all cells is 30 %.

The check-up measurements are conducted at a temperature of 25 °C. At each check-up the cells are charged up to 4.3 V with 0.5C and a constant-voltage phase of 0.05C. Afterwards a capacity measurement in discharge and charge direction is done, using a constant current of 0.5C followed by a constant-voltage phase until the current falls below 0.05C. Afterwards a quasi-OCV test with 0.1C is performed, along with severely pulse tests at 50 % SoC, which will not be discussed further in this study.

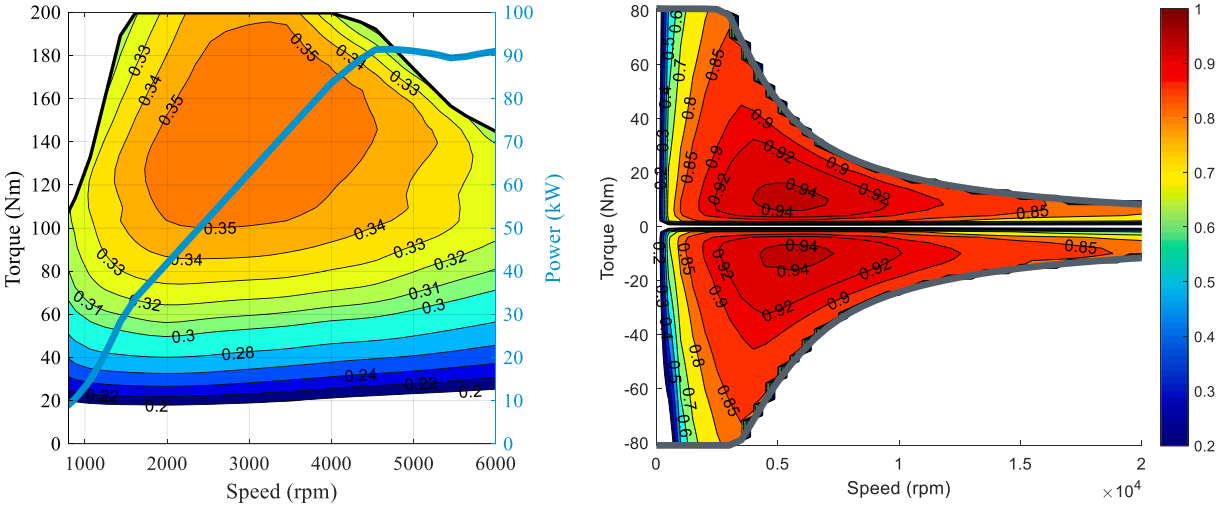

Fig. 1. Efficiency maps for (a) ICE showing the maximum torque (black) and maximum power (blue) lines and (b) EM. (For interpretation of the references to colour in this figure legend, the reader is referred to the web version of this article.)

At the end of the check-up another capacity measurement in charge and discharge direction with 0.5C is implemented. The presented capacity values are mean values of the initial and final 0.5C discharge capacity measurements to minimize the possible effects of the anode overhang during the check-up [36,37].

The calendar and cycle aging model are combined to calculate the overall capacity loss $Q_{loss,\ tot}$ as

$$Q_{loss,tot} = Q_{loss,cal} + Q_{loss,cyc} \tag{7}$$

where $Q_{loss,\ cal}$ is the capacity loss due to calendar aging and $Q_{loss,\ cyc}$ is the capacity loss induced by cyclization. A total capacity loss of 20 % is defined as the End of Life criterion in this study.

3.1. Calendar aging

To investigate the calendar aging, 9 cells were stored at three different temperatures and different SoCs. A checkup was conducted every 4 weeks to minimize the cyclization of the cell and still gain enough measurement points. The SoC is set by Ah-counting according to the measured capacity during the check-up and the voltage is kept constant afterwards.

The remaining capacity C_{cal} after calendar aging over time is modeled as

$$C_{cal} = 1 - Q_{loss,cal} \tag{8}$$

$$Q_{loss,cal} = k_{Temp,cal}(T) \cdot k_{SOC}(SOC) \cdot t^{z_{cal}} \tag{9}$$

where $k_{Temp,\ cal}$, k_{SoC} and z_{cal} are calibrated coefficients to fit the measurement results with an adopted method of [38] and t is the storage time. The measured capacity and model predictions for selected test points are shown in Fig. 2. Higher SoCs lead to accelerated aging with a nonlinear trend, which is similar to published results in [39]. The temperature dependency for the capacity loss is modeled with an widely accepted Arrhenius relationship [40–42].

Applying the calendar aging model to the hourly temperature profile of Stuttgart in Germany, shown in Fig. 3, results in a capacity loss of 3.5 % after 10 years. The required SoC profile is obtained from the year-round driving profiles while assuming that that the vehicle will get charged immediately after each driving mission. In terms of calendar aging this charging behavior leads to the most severe capacity loss as higher SoCs are harmful and consequently represents the worst case scenario. A total capacity loss of 20 % is defined as the End of Life criterion, so a loss of 16.5 % is the limit $C_{cyc,\ max}$ for cycle aging, assuming

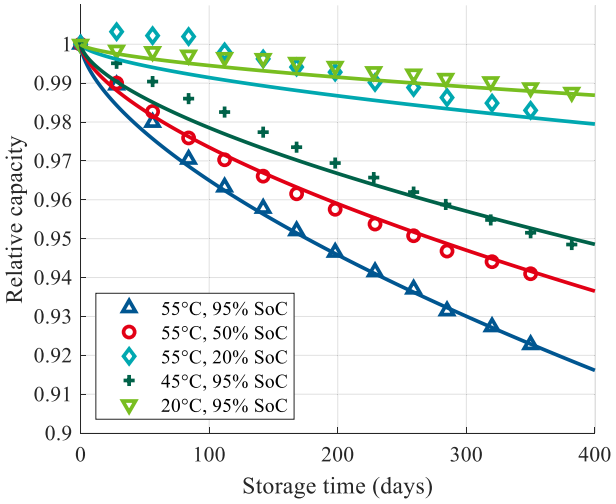

Fig. 2. Relative capacity for selected calendar aging test points. Scatter points indicate measurement values, solid lines the model predications.

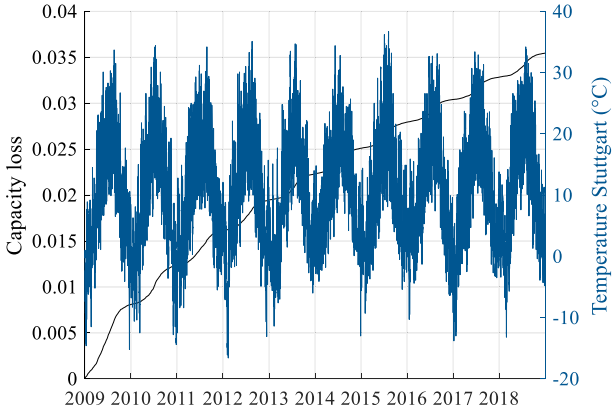

Fig. 3. Temperature profile of Stuttgart.

that there is no amplification of calendar and cycle aging in the combined model. For this battery cell, the capacity loss due to calendar aging accounts for a significant share of 17.5 % and needs to be considered during the design process.

3.2. Cycle aging

22 cells were cycled with different combinations of *DoD*, C_{dsg}, *meanSoC*, and temperature *T*. Two subsequent constant charging steps of 1C and 0.5C were chosen for all test points. Most of the test points cover different charge depleting operation scenarios, whereas one cell was cycled in charge sustaining mode with a small *DoD* of 5 % at 20 % *meanSoC* to investigate the effects of shallow cycling. The discharge rates C_{dsg} of 1C and 1.5C represent typical mean discharge scenarios for 48 V PHEVs with small battery capacities, which lead to high currents and therefore represent a worst-case scenario in terms of aging.

The relative discharge capacity over full equivalent cycles for selected test points is shown in Fig. 4. Higher discharge currents increase the battery degradation only slightly, whereas higher *DoD*s have a more significant impact. Additionally, the capacity for the cell cycled with a *DoD* of 90 % shows a strong non-linear capacity decrease after about 1000 *FEC*s. Similar curves were measured at other test points for cells cycled to an upper charging limit of 95 % *SoC*. The cells cycled with smaller *DoD*s also indicated slight nonlinear aging at the end of the measurement campaign. As temperatures of 14–18 °C were necessary to keep the cell housing temperature at a level of 25 °C, the shown behavior may be associated with the development of lithium plating. This aging mechanism is known to occur at low temperatures as well as high charging currents and has already been indicated by other studies with

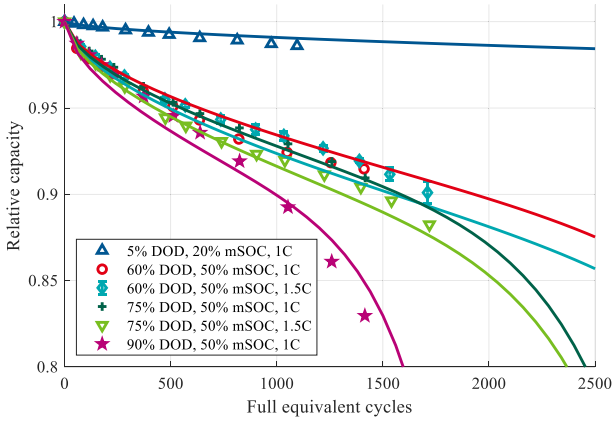

Fig. 4. Relative capacity for selected cycle aging test points. Scatter points indicate measurement values, solid lines the model predications.

similar cycling conditions [35,43]. Furthermore, the comparably high upper charging limit of 4.3 V and charging current of 1C can favor various aging mechanisms like electrolyte decomposition or cathode material losses, leading to an accelerated capacity loss [44].

The solid lines show the remaining capacity C_{cyc} after cyclization, calculated by the aging model as a function of full equivalent cycles (*FEC*)

$$C_{cyc} = 1 - Q_{loss,cyc}$$

$$Q_{loss,cyc} = Q_{loss,linear} + Q_{loss,nonlinear} \tag{10}$$

$$Q_{loss,linear} = k_{Temp,cyc}(T)\cdot k_{Crate}(Crate)\cdot k_{meanSoC}(meanSoC)\cdot k_{DoD}(DoD)\cdot FEC^{z_{cyc}} \tag{11}$$

$$Q_{loss,nonlinear} = k_{nonlinear,1}\cdot exp\left(k_{nonlinear,2}(DoD, meanSoC)\cdot FEC\right) \tag{12}$$

where $k_{Temp,\ cyc}$, k_{Crate}, $k_{meanSoC}$, k_{DoD}, $k_{nonlinear,\ 1}$, $k_{nonlinear,\ 2}$ and z_{cyc} are calibrated coefficients corresponding to the experimental parameter to fit the measurement results with a linear least square method. Even though the average discharge current of 1.5C is much higher compared to typical BEV applications, the results indicate that high-energy cells do not show severe capacity losses in these test points and are suitable for 48 V PHEV applications. For the operation mode context, it can be concluded that lower *DoDs* are beneficial in terms of capacity loss. Therefore, cyclization in charge sustaining mode leads to a smaller degradation of the cell [35,45].

The concept of a severity factor map is used to transfer the cycle aging model into the energy management strategy [46]. The severity factor σ is defined as

$$\sigma = \frac{FEC_{nom}\left(C_{dsg,nom}, meanSoC_{nom}, DoD_{nom}\right)}{FEC_{act}\left(C_{dsg}, meanSoC, DoD\right)} \tag{13}$$

Where FEC_{nom} is the number of *FEC* until the End of Life is reached with nominal conditions $meanSoC_{nom}$ and DoD_{nom}. In contrast FEC_{act} is the number of *FEC* until End of Life with the actual conditions. As the *meanSoC* and *DoD* are not known during the simulation, it is assumed that the battery will be fully discharged in the cycle. The exact capacity loss is calculated after the simulation is completed using a rainflow algorithm [47,48].

Fig. 5 shows the number of full equivalent cycles FEC_{act} until the capacity loss $C_{cyc,\ max}$ is reached during cyclization of the cells. The nominal conditions are chosen as $C_{dsg,\ nom} = 1\ C$, $meanSoC_{nom} = 0.5$, $DoD_{nom} = 0.75$ which leads to 2280 *FEC*. The steep decrease towards higher *DoDs* and *meanSoCs* reflects the previously discussed non-linear degradation effects towards high upper charging SoCs. The current dependency is modeled linearly, as only two different discharge rates are tested. For this study it is assumed that the battery temperature can be held constant at 25 °C by the cooling system.

Two additional cells are cycled with a dynamic power profile to validate the generated lifetime model. The power profile is shown in Fig. 6 which is derived from two consecutive charge depleting WLTC cycle simulations. With this profile the battery is discharged with a *DoD* of 58 % at a *meanSoC* of 50 % at begin of life. The peak discharge power of 1000 W in the validation profile results in 24 kW for the battery pack if 12 cells are connected in series and two in parallel, which is a typical range for 48 V applications. This connection results in a battery pack capacity of 9.6 kWh for the investigated cell. As the capacities in PHEVs on the market are getting larger, the peak power on cell level decreases and this profile covers the most severe power conditions.

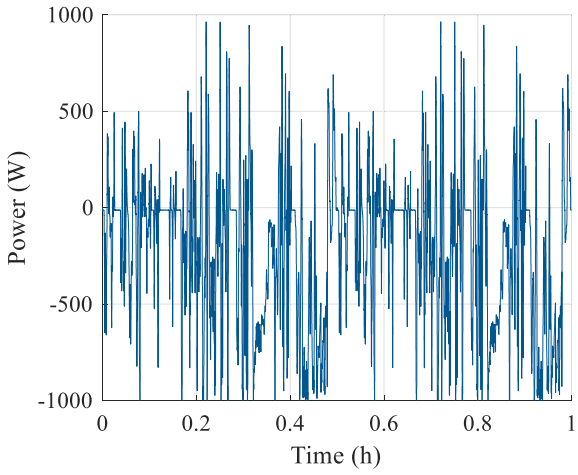

Fig. 6. Dynamic profile derived from WLTC simulation for aging model validation.

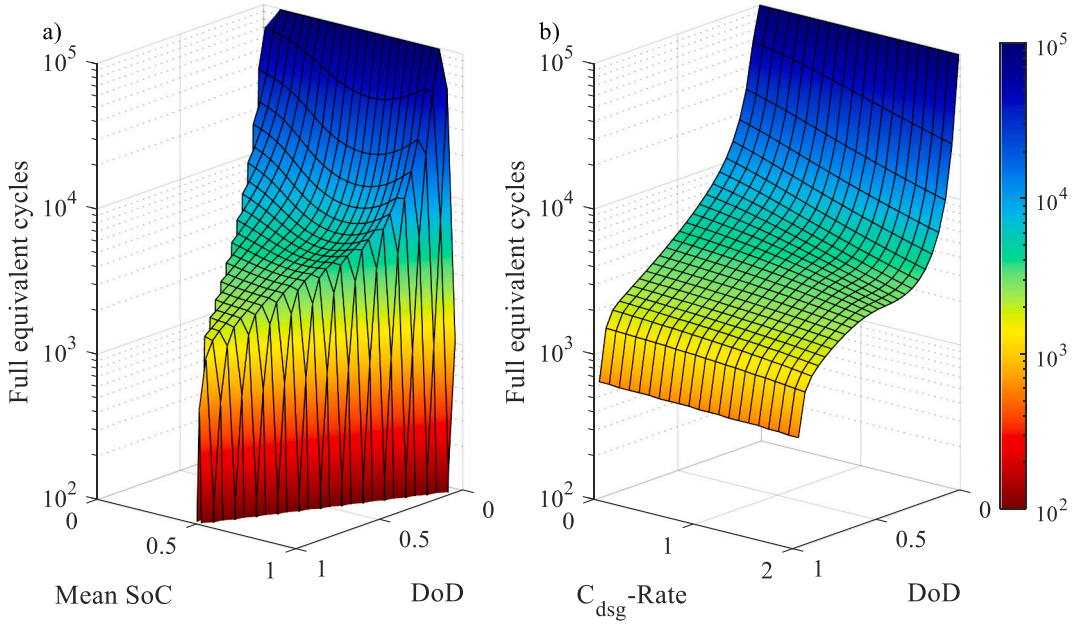

Fig. 5. Full equivalent cycles until $C_{cyc,\ max}$ is reached as a function of (a) meanSoC and DoD, (b) C_{dsg}-Rate and DoD.

The battery degradation curves for the dynamic validation profiles are shown in Fig. 7. The spread of the capacity loss is so small that the error bars are smaller than the marker size. The resistance increase remained within 5 % in the measurements and is therefore neglected in this study. The aging model can predict the capacity loss with minor deviations throughout the measurement time until about 1300 full equivalent cycles, which is equivalent to 3550 WLTC cycles. Consequently, a capacity loss of 6.6 % would be measurable after 82.000 km if the battery is used in charge depleting mode only. The validation also highlights that small recuperation pulses during dynamic cycling do not increase the capacity loss. The degradation is mainly influenced by the CC charging phase and especially the *DoD*, which is also shown [49]. Consequently, a higher energy throughput does not inevitably result in a higher capacity loss for short recuperation phases [50].

4. Optimization problem formulation

The main target of this paper is to find cost-optimal battery sizes for 48 V PHEV applications that fulfill the lifetime requirements for various customers. The aging-aware optimization workflow is shown in Fig. 8. Discrete battery pack capacities between 5 and 30 kWh are simulated with year-round drive cycles. During the sizing optimization, the number of cells connected in series is fixed to 12 to stay in a reasonable voltage range. A DP algorithm is used to find the global optimal solution for each cycle. The optimization function in this study is based on a minimization of the operational costs J as:

$$J = \int_{t_0}^{t_f} \left(c_{Fuel}\dot{m}_f + c_{Elec}P_{Bat} + \omega c_{Bat}\frac{\sigma|I_{Bat}|}{C_{Bat}FEC_{nom}} \right) dt \tag{14}$$

Where c_{Fuel} is the fuel price, c_{Elec} is the electricity price, c_{Bat} is the battery price, and ω is the weight factor for battery aging. Table 2 lists the cost parameters used in this study. The fuel and electricity prices are mean values of the five countries with the largest PHEV fleet in Europe [52]. The battery pack price is adapted, considering the base case scenario for 2025 and converted to EUR using an exchange rate of 1.09 USD/EUR. To ensure that the lifetime requirements can be met by different customers, the battery weight factor is increased until the cycle degradation is lower than $C_{cyc,\,max}$ for the cycle that results in the highest capacity loss. With the defined weight factor, the distance-weighted year-round average costs are calculated to derive the cost-optimal battery capacity.

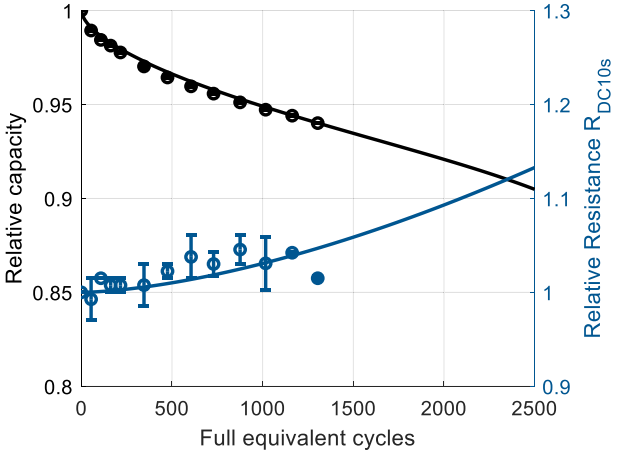

Fig. 7. Aging model validation for capacity loss and resistance increase with dynamic WLTC profile. Scatter points indicate measurement values, solid lines the model predications.

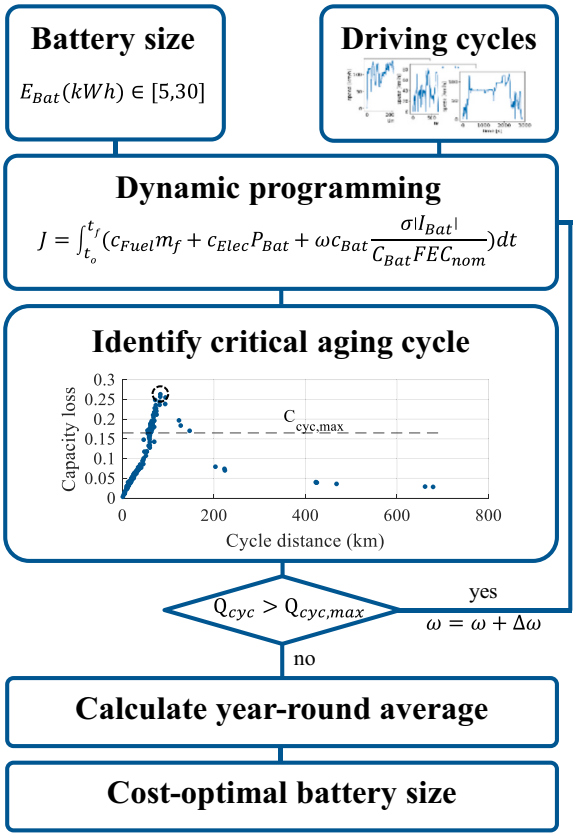

Fig. 8. Aging-aware battery sizing workflow.

Table 2
Cost parameters.

Property	Symbol	Value
Gasoline price (EUR/L) [51]	c_{Fuel}	1.93
Electricity price (EUR/kWh) [51]	c_{Elec}	0.25
Battery pack price (EUR/kWh) [53]	c_{Bat}	132

5. Simulation results and discussion

5.1. Derivation of DoD

In a first step, a suitable DoD is derived as no reference value exists in literature for this application. The capacity loss is examined for different battery capacities and DoDs in several driving cycles for this purpose. The DoD is chosen according to the most critical cycle in terms of aging to ensure that the proposed system is suitable for various types of customers.

Fig. 9a illustrates the capacity loss for different driving cycles if the DoD is fixed to 70 %. The mean SoC is set to 50 % during the optimization to have a buffer towards the upper and lower voltage limits if the battery is fully charged or discharged. The different colors represent the capacity loss for different battery capacities. It is assumed that one cycle will be repeated until the vehicle lifetime distance is reached. The aging weight factor ω is set to zero, to ensure that the lifetime requirements can be met even if the battery degradation is neglected in the operating strategy.

The largest capacity loss can be observed for small battery capacities at medium-length cycles. The dynamic and speed characteristics of the drive cycles influence the capacity loss only slightly as the spread of the markers is comparably small. First, if the battery is dimensioned smaller, the energy throughput of the cells and therefore the number of full

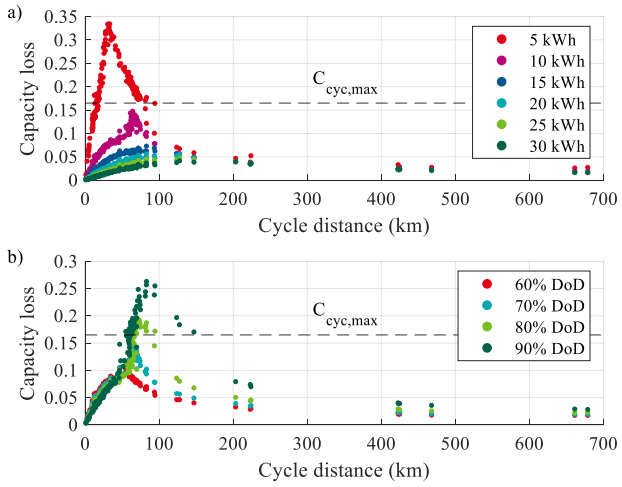

Fig. 9. Capacity loss due to cycling in different cycles with (a) a DoD of 70 % and (b) a capacity of 10 kWh.

equivalent cycles (FECs) over lifetime increases. Therefore, a lower capacity fade can be seen for larger capacities in all cycles. The second effect, the peak at medium-length cycles, is additionally influenced by the DoD. During short trips, the battery is not discharged completely, leading to a beneficial, smaller cyclization range. However, if a cycle is longer than the electric range of the vehicle, the battery is still only discharged once. Additional shallow cycles do not contribute to a capacity loss significantly. As longer cycles need to be repeated less often until the vehicle lifetime is reached, the overall capacity loss is reduced. Consequently, the capacity loss is similar for all capacities in cycles longer than 200 km as the battery is fully discharged in all cases. In summary, the largest capacity fade can be observed for cycles that exactly discharge the battery which leads to a right-shift of the peak for larger capacities.

In Fig. 9b, the influence of different DoDs for a battery capacity of 10 kWh is shown. Again, a peak can be observed for cycles that discharge the battery completely. In this case, the peak shifts towards the right because the usable capacity increases with higher DoDs. According to the presented aging model, the capacity loss increases with a higher DoD. Especially the increase from 80 % to 90 % DoD leads to a significant battery degradation because the upper charging SoC is 95 % in this case. The higher nonlinear aging share consequently results in a large capacity loss.

In realistic use-cases, commuters often travel similar distances which is specifically harmful if this distance matches the electric range of the battery. The worst case cycle is considered for the sizing optimization to ensure that the lifetime requirements for the proposed system can be fulfilled by all customers. The highest capacity losses are summarized in Table 3 where configurations, which exceed a capacity loss of $C_{cyc,\,max}$, are marked with parentheses. In these cases, the battery needs to be replaced before the vehicle reaches the EoL distance of 200.000 km. The lifetime requirements cannot be met for any of the investigated DoDs with a battery capacity of 5 kWh. For small battery sizes, the highest capacity losses occur during short cycles which need to be repeated more often, leading to a high number of FECs throughout the vehicle lifetime. With larger battery capacities the DoD can be increased so that a vehicle could be operated with a DoD of 90 % if the battery capacity exceeds 20 kWh. However, it must be noted that in this case the battery is operated close to the voltage limits of 36 V or 52 V. A DoD of 70 % is selected in the further optimization procedure as it is compatible with battery capacities of >10 kWh and allows for a buffer in the voltage limits.

Table 3
Maximum capacity loss due to cycling for different battery capacities and DoDs. Cases in parentheses indicate that the lifetime requirements cannot be met.

	Battery capacity					
DoD	5 kWh	10 kWh	15 kWh	20 kWh	25 kWh	30 kWh
60 %	(27.7 %)	10.5 %	6.9 %	5.6 %	4.7 %	4.2 %
70 %	(33.4 %)	14.7 %	7.3 %	5.6 %	4.7 %	4.2 %
80 %	(41.0 %)	(19.4 %)	7.7 %	6.2 %	5.0 %	4.7 %
90 %	(57.4 %)	(26.3 %)	(16.9 %)	7.2 %	7.0 %	5.5 %

As the average battery capacities of PHEVs in the market show an increasing trend with higher electric ranges, most of the vehicles will utilize a battery with >10 kWh which is sufficient to meet lifetime requirements with the proposed DoD of 70 %. The most critical cycle, which leads to a cyclic capacity loss of 14.7 %, would require 2871 FECs throughout the vehicle lifetime. In contrast to many commercial cells, current NMC automotive battery cells are able to exceed these requirements with a DoD of 100 % [24,25].

5.2. Aging-aware energy management strategy

In the next step, the cost reduction potential is studied if the battery degradation is considered in the energy management strategy. Fig. 10 shows the effect of different weight factors ω on the battery power. Increasing the weight factor limits the peak power of the battery which in turn increases the required ICE power and fuel consumption. The capacity loss is reduced due to two effects. First, lower currents increase the battery life according to the aging model. Second, motoric operating points are limited stronger compared to recuperation occasions, sothe battery is discharged less which reduces the DoD and energy throughput. Consequently, the battery cells endure a lower number of FECs throughout their lifetime.

The operating costs for different aging weights are shown in Fig. 11. Each capacity is simulated with the corresponding drive cycle that results in the largest capacity loss to obtain the highest aging cost-saving potential. The aging costs refer to the combined cycle and calendar degradation and the battery pack price is due if the capacity loss reaches 20 %. Similar to the findings of [54] an increasing weight factor leads to higher total operating costs as the fuel costs increase faster than the savings due to a lower capacity loss and electricity consumption in all simulated battery capacities. Nonetheless, a weight factor is necessary to fulfill the lifetime requirements for batteries smaller than 10 kWh as the combined capacity loss exceeds 20 % in red-shaded areas.

Recent cost reductions for batteries and price increases for energy carriers in the transport sector minimize the aging cost share on the overall operating cost. This is further enhanced in the case of 48 V

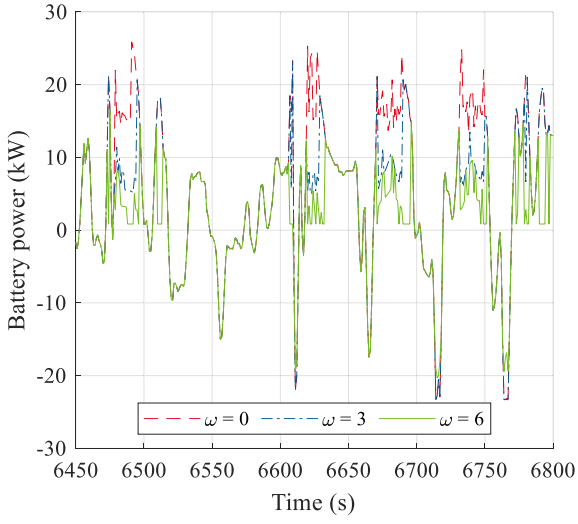

Fig. 10. Battery power limitation with increasing battery aging weight factor.

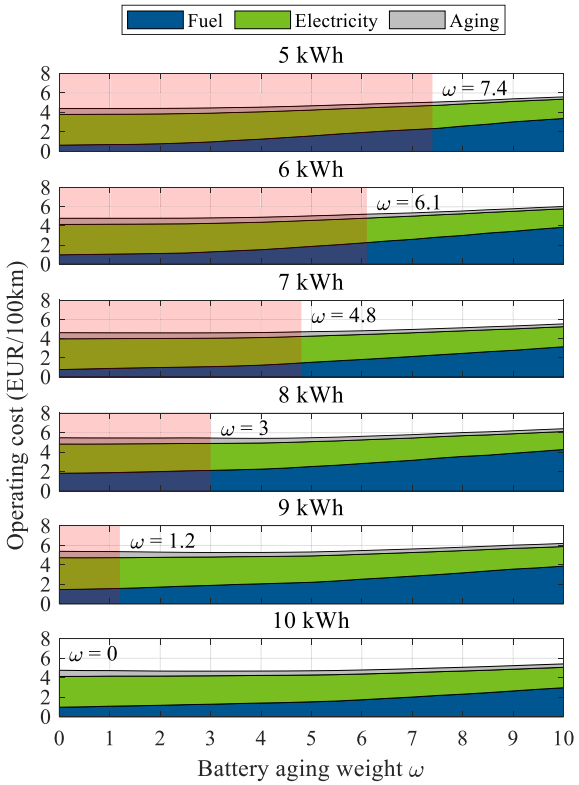

Fig. 11. Operating costs with increasing aging weight factor for different battery capacities. Each capacity is simulated with the driving cycle that results in the highest capacity loss. Red areas indicate that the lifetime requirements cannot be met. (For interpretation of the references to colour in this figure legend, the reader is referred to the web version of this article.)

PHEVs as the battery price per kWh is lower for high-energy cells compared to conventional PHEV cells. Moreover, improvements in the automotive battery cell technology allow for a large energy throughput, reducing the need for a premature replacement in many applications. In summary, the aging weight factor should be set as low as possible to achieve the lowest operating cost, which also results in the most energy-efficient solution with the lowest fuel consumption. In the following sizing optimization, the aging weight factor ω is consequently set to the smallest value for each capacity which still results in a combined capacity loss of <20 %.

5.3. Operating cost minimization

In the next step, the battery capacity is optimized to obtain the lowest operating costs. Fig. 12 shows the distance-weighted costs for the year-round driving cycles. The fuel and electricity costs account for a large part of the total costs, whereas the battery degradation cost result in a minor share. If only one specific driving cycle is considered, a minimum for the fuel costs arises when the electric range matches the drive cycle distance. The energy of larger battery capacities cannot be converted into mechanical energy and the increasing weight results in higher power demands. However, the fuel costs for the year-round cycles shrink over the complete investigated capacity range, with especially sharp decreases between 5 and 10 kWh. This highlights the need for year-round simulations in PHEV sizing studies because larger battery capacities can still decrease the overall fuel consumption, even though the energy is only beneficial in a few longer driving cycles. The electricity costs show a reverse trend because larger trip shares are covered in electric mode with higher capacities.

The aging costs show an increasing trend with a small plateau at 10 kWh. The aging weight factor reduces the battery usage between 5 and

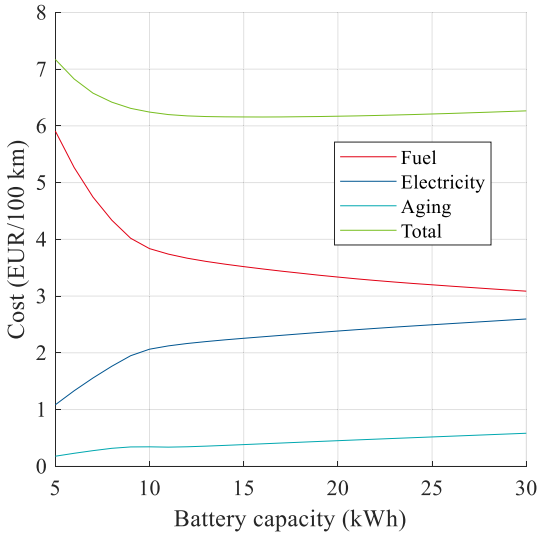

Fig. 12. Average costs over lifetime for different capacities.

10 kWh depicted by the lower aging and electricity costs. With higher capacities, the relative cycle degradation can be reduced. However, the absolute battery price increases. As shown in Fig. 9, the capacity loss can be reduced significantly up until 15 kWh and decreases only slightly with even larger capacities. Furthermore, the absolute calendar aging costs increase linearly because the capacity loss is not dependent on the battery size. The savings due to a lower cycling degradation are not sufficiently high to overcompensate for this effect. In conclusion, the combined battery aging costs show an almost linearly increasing trend.

If the three cost contributions are combined to the shown total cost curve, larger cost savings can be achieved up to 10 kWh because of the larger electrically driven trip share. Between 10 and 20 kWh the fuel savings are mostly compensated by the higher electricity costs, leading to an almost steady total cost curve. With capacities above 20 kWh, the total costs increase because the additional battery capacity cannot be used in combination with higher power requirements and increasing battery aging costs.

The optimal sizing results are compared to a 48 V HEV in Table 4. For this system, the battery cell was changed to a high power cell and the vehicle was operated in charge sustaining mode only resulting in no electricity costs. The aging calculation would require additional tests with high-power cells and is neglected. 48 V batteries in mild hybrid applications are designed for low costs with small capacities so the aging costs are expected to be low compared to the PHEV case. The total costs can be reduced by 18.5 % even for this conservative case by extending a mild hybrid to a PHEV which is charged daily. Operating the 48 V PHEV vehicle in charge sustaining mode results in a higher fuel consumption compared to the HEV case because of the larger vehicle weight. Even though the cycle aging is small due to the low DoD, the costs due to calendar aging increase the cost difference further, resulting in a total raise of 6 %.

5.4. Comparison to CO_2-optimal sizing

In our previous study [10] we derived CO_2-optimal capacities for different scenarios neglecting the battery degradation. The optimal capacity for the average driver case and a compact class vehicle, which is also used in this study, results in an optimal battery capacity of 10.2 kWh in 2020 and 22 kWh in the 2030 scenario. In future years the emissions for electricity and battery production are expected the decrease, so a larger capacity is beneficial to increase the electric driving share.

Even though the battery degradation was neglected previously, the derived capacities are above the critical limit of 10 kWh which does not

Table 4
Optimal operation cost results.

System	Capacity (kWh)	Fuel cost (EUR/100 km)	Electricity cost (EUR/100 km)	Aging cost (EUR/100 km)	Total (EUR/100 km)	Relative change
HEV	0.8	7.56	–	–	7.56	–
PHEV cs	16	7.82	–	0.19	8.01	+ 6.0 %
PHEV	16	3.48	2.28	0.40	6.16	- 18.5 %

require the inclusion of a battery weight factor. The proposed system should therefore be expected to fulfill the lifetime requirements as well.

The cost-optimal capacity proposed in this study is located exactly within this range. The total cost curve is found to be relatively flat, meaning that larger battery capacities, which are CO_2-optimal in future years and drivers with a higher annual mileage, result in a minor cost increase.

6. Summary and outlook

This paper presents a cost-optimal battery sizing method for 48 V PHEVs which includes the degradation of the battery cells. As the parametrized battery cells of the widely used semi-empirical aging models found in literature do not fit to the requirements of 48 V PHEVs, the results of the conducted calendar and cycling aging experiments for an automotive high-energy cell are presented. The generated semi-empirical model is implemented into the DP optimization framework to define a system layout that fulfills the lifetime requirements. The key findings are:

(1) With the assumed conditions, the capacity loss during calendar aging was found to be 3.5 % which results in a share of at least 17.5 % if the total capacity loss of 20 % is reached. Therefore, it should be considered during the design process to meet the lifetime requirements and find the cost-optimal result.
(2) The cycle aging model revealed that smaller DoDs do not contribute to the overall capacity loss, so only the main discharge process is relevant. Furthermore, avoiding high charging SoCs is recommended due to the risk of accelerated, non-linear capacity loss.
(3) The aging weight factor reduces the peak C-rates and energy throughput of the battery cells, which can increase the battery lifetime. However, the factor should be set as low as possible because the increasing fuel consumption leads to higher costs and CO_2 emissions. The contribution of the battery aging costs is low compared to the fuel and electricity costs.
(4) The simulation of year-round driving profiles showed that the lifetime costs are minimized at 16 kWh but are almost insensitive to the battery capacity above 10 kWh. The fuel consumption and electricity cost showed no peak, indicating that large battery capacities are beneficial even though the energy can be used in only a few longer drive cycles under the assumption of frequent charging.

The implementation of the proposed system still needs to be investigated and optimized in real-time applications with online EMSs. The publication of comprehensive battery aging experiments and subsequent derivation of semi-empirical aging models for current high-energy cells can improve the accuracy of the capacity loss predictions. Furthermore, the thermal effects and ambient conditions should be studied in detail, along with on-road vehicle verification tests.

Declaration of competing interest

The authors declare that they have no known competing financial interests or personal relationships that could have appeared to influence the work reported in this paper.

Data availability

The authors do not have permission to share data.

References

[1] X. Hu, J. Han, X. Tang, X. Lin, Powertrain design and control in electrified vehicles: a critical review, IEEE Trans.Transp.Electrification (2021), https://doi.org/10.1109/TTE.2021.3056432.
[2] X. Hu, Y. Zou, Y. Yang, Greener plug-in hybrid electric vehicles incorporating renewable energy and rapid system optimization, Energy 111 (12) (2016) 971–980, https://doi.org/10.1016/j.energy.2016.06.037.
[3] J. Tu, Z. Bai, X. Wu, Sizing of a plug-in hybrid electric vehicle with the hybrid energy storage system, WEVJ 13 (7) (2022) 110, https://doi.org/10.3390/wevj13070110.
[4] X. Shaobo, Z. Qiankun, H. Xiaosong, L. Yonggang, L. Xianke, Battery sizing for plug-in hybrid electric buses considering variable route lengths, Energy (2021) 226, https://doi.org/10.1016/j.energy.2021.120368.
[5] H. Basma, C. Mansour, M. Haddad, M. Nemer, P. Stabat, Energy consumption and battery sizing for different types of electric bus service, Energy 239 (May) (2022), 122454, https://doi.org/10.1016/j.energy.2021.122454.
[6] S. Xie, X. Hu, Q. Zhang, X. Lin, B. Mu, H. Ji, Aging-aware co-optimization of battery size, depth of discharge, and energy management for plug-in hybrid electric vehicles, J. Power Sources (2020) 450, https://doi.org/10.1016/j.jpowsour.2019.227638.
[7] S. Lauer, M. Perugini, R. Weldle, F. Graf, 48 volt high power – much more than a mild hybrid, in: 29th Aachen Colloquium Sustainable Mobility 2020. Aachen, 2020.
[8] S. Lauer, R. Weldle, M. Perugini, A. Lyubar, 48-V high-power full hybrid system, MTZ Worldw. 82 (2) (2021) 24–31, https://doi.org/10.1007/s38313-020-0592-0.
[9] P. Kapus, M. Brendel, G. Teuschl, T. Pels, 48-V plug-in hybrid vehicles for inner-city zero emission, ATZ Worldw. 121 (10) (2019) 26–33, https://doi.org/10.1007/s38311-019-0108-1.
[10] T. Frambach, R. Kleisch, R. Liedtke, J. Schwarzer, E. Figgemeier, Environmental impact assessment and classification of 48 V plug-in hybrids with real-driving use case simulations, Energies 15 (7) (2022) 2403, https://doi.org/10.3390/en15072403.
[11] M. Safoutin, B. Ellies, J. McDonald, Predicting the Future Manufacturing Cost of Batteries for Plug-in Vehicles for the U.S. Environmental Protection Agency (EPA) 2017–2025 Light-Duty Greenhouse Gas Standards, WEVJ 9 (3) (2018) 42, https://doi.org/10.3390/wevj9030042.
[12] G. Zubi, R.S. Adhikari, N.E. Sánchez, W. Acuña-Bravo, Lithium-ion battery-packs for solar home systems: layout, cost and implementation perspectives, J.Energy Storage 32 (2) (2020), 101985, https://doi.org/10.1016/j.est.2020.101985.
[13] M. Pourabdollah, N. Murgovski, A. Grauers, B. Egardt, Optimal sizing of a parallel PHEV powertrain, IEEE Trans. Veh. Technol. 62 (6) (2013) 2469–2480, https://doi.org/10.1109/TVT.2013.2240326.
[14] M. Redelbach, E.D. Özdemir, H.E. Friedrich, Optimizing battery sizes of plug-in hybrid and extended range electric vehicles for different user types, Energy Policy 73 (2014) 158–168, https://doi.org/10.1016/j.enpol.2014.05.052.
[15] D.-D. Tran, M. Vafaeipour, M. El Baghdadi, R. Barrero, J. van Mierlo, O. Hegazy, Thorough state-of-the-art analysis of electric and hybrid vehicle powertrains: topologies and integrated energy management strategies, Renew. Sust. Energ. Rev. 119 (2020) 1–29, https://doi.org/10.1016/j.rser.2019.109596.
[16] N. Sockeel, J. Shi, M. Shahverdi, M. Mazzola, Pareto front analysis of the objective function in model predictive control based power management system of a plug-in hybrid electric vehicle, in: 2018 IEEE Transportation Electrification Conference and Expo (ITEC), 2018, pp. 971–976, https://doi.org/10.1109/ITEC.2018.8449957.
[17] M. Mahmoodi-k, M. Montazeri-Gh, V. Madanipour, Simultaneous multi-objective optimization of a PHEV power management system and component sizing in real world traffic condition, Energy 223 (2021), https://doi.org/10.1016/j.energy.2021.121111.
[18] Y. Huang, H. Wang, A. Khajepour, B. Li, J. Ji, K. Zhao, et al., A review of power management strategies and component sizing methods for hybrid vehicles, Renew. Sust. Energ. Rev. 96 (2018) 132–144, https://doi.org/10.1016/j.rser.2018.07.020.
[19] Z. Chen, J. Lu, B. Liu, N. Zhou, S. Li, Optimal energy management of plug-in hybrid electric vehicles concerning the entire lifespan of lithium-ion batteries, Energies 13 (10) (2020) 1–15, https://doi.org/10.3390/en13102543.
[20] J.A. López-Ibarra, H. Gaztañaga, A. Saez-de-Ibarra, H. Camblong, Plug-in hybrid electric buses total cost of ownership optimization at fleet level based on battery aging, Appl. Energy 280 (2020) 1–15, https://doi.org/10.1016/j.apenergy.2020.115887.

[21] S. Zhou, Z. Chen, D. Huang, T. Lin, Model prediction and rule based energy management strategy for a plug-in hybrid electric vehicle with hybrid energy storage system, IEEE Trans. Power Electron. 36 (5) (2021) 5926–5940, https://doi.org/10.1109/TPEL.2020.3028154.
[22] Y. He, C. Wang, Q. Zhou, J. Li, M. Makridis, H. Williams, et al., Multiobjective component sizing of a hybrid ethanol-electric vehicle propulsion system, Appl. Energy 266 (2020), 114843, https://doi.org/10.1016/j.apenergy.2020.114843.
[23] Y. Bai, J. Li, H. He, R.C.D. Santos, Q. Yang, Optimal design of a hybrid energy storage system in a plug-in hybrid electric vehicle for battery lifetime improvement, IEEE Access 8 (2020) 142148–142158, https://doi.org/10.1109/ACCESS.2020.3013596.
[24] P. Daubinger, M. Schelter, R. Petersohn, F. Nagler, S. Hartmann, M. Herrmann, et al., Impact of bracing on large format prismatic lithium-ion battery cells during aging, Adv. Energy Mater. 12 (10) (2022), 2102448, https://doi.org/10.1002/aenm.202102448.
[25] J.E. Harlow, X. Ma, J. Li, E. Logan, Y. Liu, N. Zhang, et al., A wide range of testing results on an excellent lithium-ion cell chemistry to be used as benchmarks for new battery technologies, J. Electrochem. Soc. 166 (13) (2019) A3031, https://doi.org/10.1149/2.0981913jes.
[26] Y. Liang, S. Makam, PHEV hybrid vehicle system efficiency and battery aging optimization using A-ECMS based algorithms, SAE Int. (2020) 1–9, https://doi.org/10.4271/2020-01-1178.
[27] X. Zhang, L. Guo, N. Guo, Y. Zou, G. Du, Bi-level energy management of plug-in hybrid electric vehicles for fuel economy and battery lifetime with intelligent state-of-charge reference, J. Power Sources 481 (6) (2021), 228798, https://doi.org/10.1016/j.jpowsour.2020.228798.
[28] N. Guo, X. Zhang, Y. Zou, L. Guo, G. Du, Real-time predictive energy management of plug-in hybrid electric vehicles for coordination of fuel economy and battery degradation, Energy 214 (2021) 1–20, https://doi.org/10.1016/j.energy.2020.119070.
[29] X. Zhang, Y. Gao, B. Guo, C. Zhu, X. Zhou, L. Wang, et al., A novel quantitative electrochemical aging model considering side reactions for lithium-ion batteries, Electrochim. Acta 343 (8) (2020), 136070, https://doi.org/10.1016/j.electacta.2020.136070.
[30] S.J. Moura, J.L. Stein, H.K. Fathy, Battery-health conscious power management in plug-in hybrid electric vehicles via electrochemical modeling and stochastic control, IEEE Trans. Contr. Syst. Technol. 21 (3) (2013) 679–694, https://doi.org/10.1109/TCST.2012.2189773.
[31] J. Schmalstieg, S. Käbitz, M. Ecker, D.U. Sauer, A holistic aging model for Li(NiMnCo)O2 based 18650 lithium-ion batteries, J. Power Sources 257 (2014) 325–334, https://doi.org/10.1016/j.jpowsour.2014.02.012.
[32] G. Suri, S. Onori, A control-oriented cycle-life model for hybrid electric vehicle lithium-ion batteries, Energy 96 (2016) 644–653, https://doi.org/10.1016/j.energy.2015.11.075.
[33] J. Wang, P. Liu, J. Hicks-Garner, E. Sherman, S. Soukiazian, M. Verbrugge, et al., Cycle-life model for graphite-LiFePO{$_4$} cells, J. Power Sources 196 (8) (2011) 3942–3948, https://doi.org/10.1016/j.jpowsour.2010.11.134.
[34] T. Frambach, R. Liedtke, P. Dechent, D.U. Sauer, E. Figgemeier, A review on aging-aware system simulation for plug-in hybrids, IEEE Trans. Transp. Electrific. 8 (2) (2022) 1524–1540, https://doi.org/10.1109/TTE.2021.3104105.
[35] J. Stadler, C. Krupp, M. Ecker, J. Bandlow, B. Spier, A. Latz, Investigation and modeling of cyclic aging using a design of experiment with automotive grade lithium-ion cells, J. Power Sources 521 (2022), 230952, https://doi.org/10.1016/j.jpowsour.2021.230952.
[36] M. Naumann, F.B. Spingler, A. Jossen, Analysis and modeling of cycle aging of a commercial LiFePO4/graphite cell, J. Power Sources 451 (14) (2020), 227666, https://doi.org/10.1016/j.jpowsour.2019.227666.
[37] J. Wilhelm, S. Seidlmayer, P. Keil, J. Schuster, A. Kriele, R. Gilles, et al., Cycling capacity recovery effect: a coulombic efficiency and post-mortem study, J. Power Sources 365 (2017) 327–338, https://doi.org/10.1016/j.jpowsour.2017.08.090.
[38] M. Naumann, M. Schimpe, P. Keil, H.C. Hesse, A. Jossen, Analysis and modeling of calendar aging of a commercial LiFePO4/graphite cell, J.Energy Storage 17 (2018) 153–169, https://doi.org/10.1016/j.est.2018.01.019.
[39] D. Werner, S. Paarmann, T. Wetzel, Calendar aging of Li-ion cells—experimental investigation and empirical correlation, Batteries 7 (2) (2021) 1–24, https://doi.org/10.3390/batteries7020028.
[40] M. Ecker, N. Nieto, S. Käbitz, J. Schmalstieg, H. Blanke, A. Warnecke, et al., Calendar and cycle life study of Li(NiMnCo)O2-based 18650 lithium-ion batteries, J. Power Sources 248 (2014) 839–851, https://doi.org/10.1016/j.jpowsour.2013.09.143.
[41] S. Käbitz, J.B. Gerschler, M. Ecker, Y. Yurdagel, B. Emmermacher, D. André, et al., Cycle and calendar life study of a graphite|LiNi1/3Mn1/3Co1/3O2 Li-ion high energy system. Part A: full cell characterization, J. Power Sources 239 (2013) 572–583, https://doi.org/10.1016/j.jpowsour.2013.03.045.
[42] M.S. Hosen, D. Karimi, T. Kalogiannis, A. Pirooz, J. Jaguemont, M. Berecibar, et al., Electro-aging model development of nickel-manganese-cobalt lithium-ion technology validated with light and heavy-duty real-life profiles, J.Energy Storage 28 (2020), 101265, https://doi.org/10.1016/j.est.2020.101265.
[43] T. Waldmann, B.-I. Hogg, M. Wohlfahrt-Mehrens, Li plating as unwanted side reaction in commercial Li-ion cells – a review, J. Power Sources 384 (2018) 107–124, https://doi.org/10.1016/j.jpowsour.2018.02.063.
[44] W.M. Dose, C. Xu, C.P. Grey, M.F.L. de Volder, Effect of anode slippage on cathode cutoff potential and degradation mechanisms in Ni-rich Li-ion batteries, Cell Rep. Phys.Sci. 1 (11) (2020), 100253, https://doi.org/10.1016/j.xcrp.2020.100253.
[45] M. Lewerenz, C. Rahe, G. Fuchs, C. Endisch, D.U. Sauer, Evaluation of shallow cycling on two types of uncompressed automotive Li(Ni1/3Mn1/3Co1/3)O2-graphite pouch cells, J.Energy Storage 30 (2020), 101529, https://doi.org/10.1016/j.est.2020.101529.
[46] S. Onori, P. Spagnol, V. Marano, Y. Guezennec, G. Rizzoni, A new life estimation method for lithium-ion batteries in plug-in hybrid electric vehicles applications, J. Power Electron. (2012) 302–319.
[47] D. Fioriti, L. Pellegrino, G. Lutzemberger, E. Micolano, D. Poli, Optimal sizing of residential battery systems with multi-year dynamics and a novel rainflow-based model of storage degradation: an extensive Italian case study, Electr. Power Syst. Res. 203 (1–2) (2022), 107675, https://doi.org/10.1016/j.epsr.2021.107675.
[48] J. de Hoog, J.-M. Timmermans, D. Ioan-Stroe, M. Swierczynski, J. Jaguemont, S. Goutam, et al., Combined cycling and calendar capacity fade modeling of a nickel-manganese-cobalt oxide cell with real-life profile validation, Appl. Energy 200 (2017) 47–61, https://doi.org/10.1016/j.apenergy.2017.05.018.
[49] P. Keil, A. Jossen, Impact of dynamic driving loads and regenerative braking on the aging of lithium-ion batteries in electric vehicles, J. Electrochem. Soc. 164 (13) (2017) A3081, https://doi.org/10.1149/2.0801713jes.
[50] R. Wegmann, V. Döge, D.U. Sauer, Assessing the potential of a hybrid battery system to reduce battery aging in an electric vehicle by studying the cycle life of a graphite|NCA high energy and a LTO|metal oxide high power battery cell considering realistic test profiles, Appl. Energy 226 (2018) 197–212, https://doi.org/10.1016/j.apenergy.2018.05.104.
[51] Global Petrol Prices, Available from: https://www.globalpetrolprices.com/, April 25, 2022.
[52] European Commission, European Alternative Fuels Observatory (EAFO), Available from:, April 25, 2022 https://alternative-fuels-observatory.ec.europa.eu/.
[53] I.-Y.L. Hsieh, M.S. Pan, Y.-M. Chiang, W.H. Green, Learning only buys you so much: practical limits on battery price reduction, Appl. Energy 239 (2019) 218–224, https://doi.org/10.1016/j.apenergy.2019.01.138.
[54] S. Zhang, X. Hu, S. Xie, Z. Song, L. Hu, C. Hou, Adaptively coordinated optimization of battery aging and energy management in plug-in hybrid electric buses, Appl. Energy 256 (2019), 113891, https://doi.org/10.1016/j.apenergy.2019.113891.